Dielectric Properties and Structures of Melt-Compounded Poly(ethylene oxide)–Montmorillonite Nanocomposites

Shobhna Choudhary, R. J. Sengwa

Dielectric Research Laboratory, Department of Physics, J N V University, Jodhpur 342 005, India

Received 13 May 2011; accepted 30 August 2011
DOI 10.1002/app.35556
Published online 7 December 2011 in Wiley Online Library (wileyonlinelibrary.com).

ABSTRACT: The dielectric dispersion and relaxation process in melt-compounded hot-pressed poly(ethylene oxide) (PEO)–montmorillonite (MMT) clay nanocomposite films of 0–20 wt % MMT concentration were investigated over the frequency range 20 Hz to 1 MHz at ambient temperature. X-ray diffraction study of the nanocomposites evidences that the PEO has been intercalated into the MMT interlayer galleries with a helical-type multilayer structures, which results the formation of unique parallel plane PEO–MMT layered structures. The relaxation times corresponding to PEO chain segmental motion were determined from the loss peak frequencies of different dielectric formalisms and the same is used to explore the interactions compatibility between PEO molecules and the MMT nano platelets. It is revealed that the loading of only 1 wt % MMT in PEO matrix significantly increases the PEO chain segmental motion due to intercalation, which further varies anomalously with increase of MMT concentration. The real part of dielectric function at 1 MHz, relaxation time, and dc conductivity of these melt-compounded nanocomposites were compared with the aqueous solution-cast PEO–MMT films. Considering the comparative changes in the values of various dielectric parameters, the effect of synthesization route on the intercalated/exfoliated-MMT structures and the PEO chain dynamics were discussed. © 2011 Wiley Periodicals, Inc. J Appl Polym Sci 124: 4847–4853, 2012

Key words: poly(ethylene oxide); MMT clay; nanocomposites; dielectric relaxation; electrical conductivity

INTRODUCTION

The last two decades have a tremendous investigations on the solution-cast and melt-compounded poly(ethylene oxide) (PEO)–montmorillonite (MMT) nanocomposites in view of their academic interest and potential applications in nanomaterial technology.[1–8] MMT is 2 : 1 charged phyllosilicates sheets of 1 nm thickness and stacked by weak dipolar or van der Waals forces, leading to the intercalation of water or polar organic molecules and causing the crystal lattice to expand in the *c* direction. The linear chain polar PEO and MMT have hydrophilic properties due to which the PEO partially adsorbs on the MMT-platelets surfaces besides the intercalation in MMT galleries. The characterization of PEO–MMT nanocomposites by different spectroscopic, morphological, and physical techniques established that the loading of MMT in PEO matrix substantially improves the mechanical, thermal, optical, chemical, and gas permeable properties when compared with pure PEO film. These properties are mainly governed by the interactions compatibility at a molecular level between the PEO and the intercalated/exfoliated-MMT structures of the nanocomposites.

The broadband dielectric relaxation spectroscopy of the colloids and films of polymer clay nanocomposite (PCN) materials have established its potential use for the conformation of clay structures and polymer chain dynamics.[9–25] The characterization of dielectric parameters of melt-compounded PCN materials have also attracted a lot of attention in online process monitoring and offline measurements.[9,11,13] Further, the synthesization of novel PCN insulators of low dielectric constant and loss with improved physical properties has been a pressing demand for the suitable substrate materials in integrated electronic circuits and the membrane technology,[22–30] and also in solid state electrolytes.[31–33] The survey reveals that the dielectric/electrical properties of PEO–MMT nanocomposites prepared by melt-compounded technique have not been well studied and deserves their detailed exploration.

Taking into consideration the above facts, in the present article an attempt is made to investigate the dielectric/electrical properties of the melt-compounded PEO–MMT nanocomposite films and the results were compared with their solution-cast films. The variation in values of dielectric parameters with increase of MMT concentration and their correlation with the intercalated/exfoliated-MMT structures of the PEO–MMT nanocomposite prepared by different routes

Correspondence to: R. J. Sengwa (rjsengwa@rediffmail.com).

were explored. The PEO–MMT intercalated structures were also characterized by X-ray diffraction (XRD) measurements and compared with the structural findings based on their dielectric properties.

EXPERIMENTAL

Materials

The PEO of molecular weight 600,000 g/mol and polymer grade hydrophilic MMT (Nanoclay, PGV), a product of Nanocor®, were purchased from Sigma-Aldrich, USA. The MMT is white in color, and has 145 meq/100 g cation exchange capacity, 150–200 aspect ratio, 2.6 g/cc specific gravity and 9–10 pH value on 5% dispersion.

Preparation of PEO–MMT nanocomposite films

First, the required amounts of PEO (4.00, 3.96, 3.92, 3.88, 3.80, 3.60, and 3.20 g), and respective amounts of MMT (0.00, 0.04, 0.08, 0.12, 0.20, 0.40, and 0.80 g) of 4 g total weight of PEO + MMT for the 0, 1, 2, 3, 5, 10, and 20 wt % MMT, respectively, were mechanically mixed using an agate mortar and pestle. After that melt-compounded films of each PEO–MMT mixture were obtained by heating the material for 20 min duration at 70°C under 3 tons of pressure in 60 mm diameter stainless steel die having 1-mm spacer using hot-press polymer film making unit. The films synthesization temperature was kept slightly higher than the melting temperature of PEO, i.e., 65°C for the proper melt of PEO and its mixing with MMT.

Measurements

Agilent 4284A precision LCR meter and Agilent 16451B solid dielectric test fixture having a four terminals nickel-plated cobalt (an alloy of 17% cobalt + 29% nickel + 54% iron) electrodes of diameter 38 mm, were used for the dielectric/electrical characterization of the PEO–MMT films in the frequency range 20 Hz to 1 MHz. Frequency dependent values of parallel capacitance C_P, parallel resistance R_p, and loss tangent tanδ (dissipation factor D) of the dielectric test fixture used as a capacitor filled with the PEO–MMT films, were measured at ambient temperature (30°C). Prior to the sample measurements, the open-circuit calibration of the dielectric test fixture was performed to eliminate the effect of stray capacitance. The equations used for the evaluation of complex dielectric function $\varepsilon^*(\omega) = \varepsilon' - j\varepsilon''$, complex alternating current (AC) electrical conductivity $\sigma^*(\omega) = \sigma' + j\sigma''$, complex electric modulus $M^*(\omega) = M' + jM''$, and complex impedance $Z^*(\omega) = Z' - jZ''$ of the nanocomposite films are same as described earlier.[23]

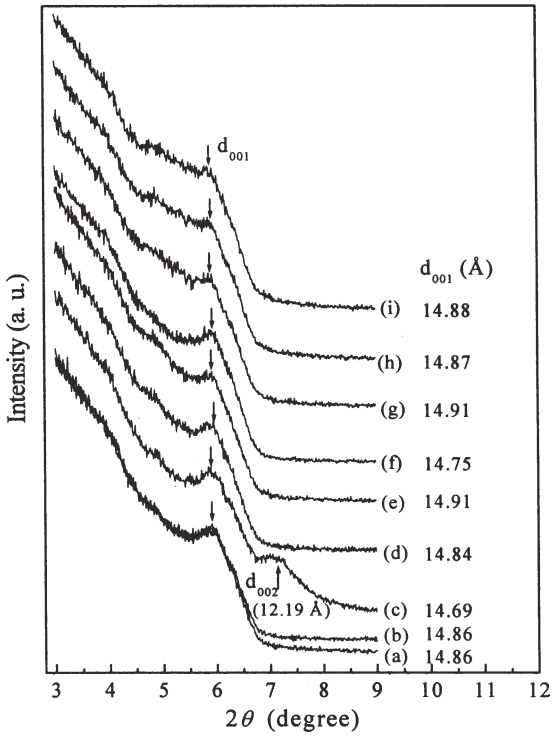

Figure 1 XRD patterns of melt-compounded PEO–MMT nanocomposite films at varying MMT concentration (wt %): (a) PEO powder, (b) melt PEO film, (c) MMT powder, (d) 1 wt % MMT, (e) 2 wt % MMT, (f) 3 wt % MMT, (g) 5 wt % MMT, (h) 10 wt % MMT, and (i) 20 wt % MMT.

The XRD patterns of PEO, MMT, and PEO–MMT nanocomposites were recorded using a PANalytical X'pert Pro MPD diffractometer of Cu Kα radiation (1.5406 Å) operated at 45 kV and 40 mA with a scanned step size of 0.01° and time for each step 2 s.

RESULTS AND DISCUSSION

XRD analysis

The XRD patterns in a 2θ (Bragg angles) range 3–9° of PEO powder, melt PEO film, MMT powder, and melt-compounded PEO–MMT nanocomposite films of various MMT concentration are depicted in Figure 1. The PEO powder and melt-synthesized PEO film have good resemblance in their XRD patterns. The observed broader peak at 2θ = 5.9368° corresponds to the bulk PEO matrix, because the crystalline phase of PEO major peaks occur at ~ 19.5 and 23.5°.[33] Earlier, the broader peak at same 2θ position for PEO matrix was also reported.[34] The semicrystalline PEO has an arrangement of the lamellar nanostructure,[6] and the observed peak represents the inter-lamellar spacing in PEO matrix (the basal plane d-spacing). The XRD pattern of pristine MMT has two broader peaks at 2θ = 6.0139° and 7.2476°, corresponds to the 001 and 002 d-spacing,

respectively, which are consistent with the earlier findings.[5,35–37]

On addition of MMT in the PEO matrix, there is a change in peak position, peak width, and peak intensity of XRD patterns, which relates to a change of the location of d_{001} peak. The values of d_{001}-spacing indexed as indicated on the XRD patterns were determined using the Bragg's relation $\lambda = 2d\sin\theta$, where λ corresponds to the wavelength of X-ray radiation ($\lambda = 1.5406$ Å) of the diffractometer, d is the spacing between diffractional lattice planes, and θ is the measured diffraction angle. The large value of d_{001}-spacing (14.69 Å) and hydrophilic behavior of pristine MMT favors the direct intercalation of linear chain polar PEO molecules in the MMT galleries, because the thickness of PEO helical structure is ~ 4 Å.[38] Figure 1 shows that for PEO–MMT nanocomposites, a small peak shift toward the lower-angle side is an evidence of the increase in d_{001}-spacing (MMT gallery width) when compared with that of pure MMT, which confirms the intercalation of PEO, although XRD alone cannot be used to indicate the extent of intercalation. Further, in all the PEO–MMT nanocomposites d_{002} peak of pure MMT disappeared, which indicates the partial adsorption of PEO on the exfoliated MMT platelets surfaces. A very small change in d_{001} of PEO–MMT nanocomposites with increase of MMT concentration demonstrates that the thickness of intercalated layers of PEO in MMT galleries remains same in the melt-compounded nanocomposites, which may be due to their synthesization under pressure. The significant decrease in relative intensity of d_{001} peaks for MMT concentrations greater than 5 wt % indicates the decrease in the degree of crystallinity of PEO matrix, which is owing to the disruptions of the spatial continuity of the lamellae arrangement of large intercalated PEO chain.[6] The same values of d_{001}-spacing of PEO–MMT nanocomposite also confirms that the melt intercalation under pressure appears more likely to be one-step process, and support a helical or multilayer trans–gauche–trans (*tgt*) structure of PEO in the MMT galleries with their parallel plane structures, as revealed by the earlier findings.[2,5,6]

Complex dielectric spectra

Figure 2 shows that the ε′ values of melt-compounded PEO–MMT nanocomposite films initially decrease with increase of frequency and attain the constant values near 1 MHz. The inset of Figure 2 indicates that the ε′ values at 1 MHz of these nanocomposites vary anomalously with increase of MMT concentration. The change in ε′ values of PCNs have strong correlation with intercalated/exfoliated structures of MMT in the polymer matrix.[7,9–27] It has been established that for the PCN, the predominance

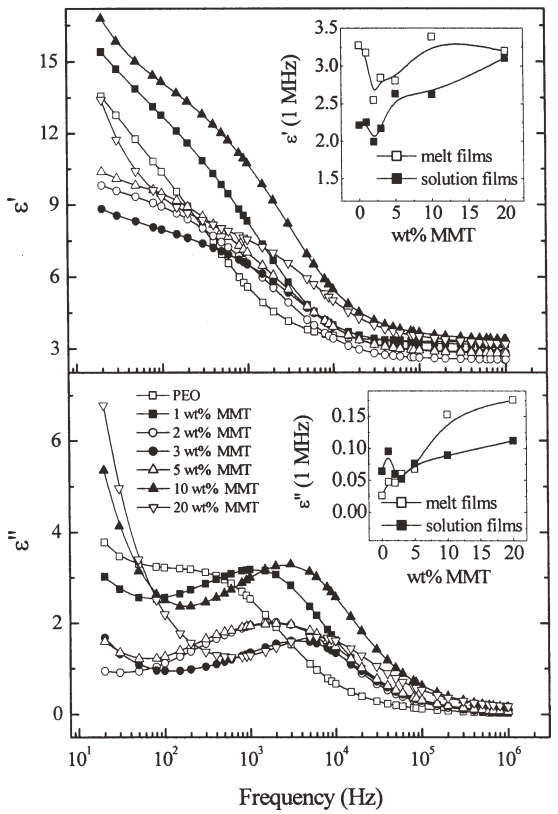

Figure 2 Frequency dependence of real part ε′ and loss ε″ of dielectric function of the melt-compounded PEO–MMT nanocomposite films at varying MMT concentration (wt %). Insets show the MMT concentration (wt %) dependence of ε′ and ε″ at 1 MHz of melt-compounded and aqueous solution-cast PEO–MMT films.

of exfoliated-MMT structure in the polymer matrix decreases the ε′ values, whereas large amount of intercalated structure increases it.[9,11,12–15,22–26]

The XRD study of PEO–MMT nanocomposites (Fig. 1) revealed that due to hydrophilic behavior of the PEO and MMT, the long chain PEO molecules intercalate in MMT galleries, which is influenced by the MMT concentration, and also governed by the nanocomposite preparation route.[2,3] When compared with pure PEO, the low ε′ values at 1 MHz of the PEO–MMT up to 5 wt % MMT (inset of Fig. 2) confirms the predominance of MMT-exfoliated structure. At 2 wt % MMT, the maximum decrease in ε′ value is the evidence of the formation of comparative large amount of MMT-exfoliated structure in melt-compounded PEO–MMT film. The ε′ values at 10 and 20 wt % MMT are found nearly equal to that of the pure PEO film, which suggests that the exfoliated- and intercalated-MMT structures are formed almost in equal amount at these concentrations and these results are in agreement with their XRD analysis. Inset of Figure 2 also included the ε′ values at 1 MHz of the aqueous solution-cast PEO–MMT films,[25] which are low when compared with that of

the melt-compounded films but have the similar type of variation with the increase of MMT concentration. These comparative ε′ values reveal that the structures of PEO–MMT nanocomposites depend on their preparation route. Further, the ε′ values at 1 MHz are in the range of 2–3.5, confirms the suitability of these low dielectric constant materials in the radiowave device technology, because they also have low value of dielectric loss at 1 MHz (inset of Fig. 2).

The ε″ spectra of the PEO–MMT films (Fig. 2) have relaxation peaks in the frequency range 100 Hz to 10 kHz, which correspond to PEO segmental motion (local chain motion of PEO). The values of PEO segmental motion dielectric relaxation time τ_ε of these nanocomposite films were evaluated from the dielectric loss peak frequency $f_{p(\varepsilon'')}$ using the relation $\tau_\varepsilon = (2\pi f_{p(\varepsilon'')})^{-1}$. The inset of Figure 2 also shows the comparison of ε″ values at 1 MHz of the melt-compounded PEO–MMT films with their aqueous solution-cast films.[25] It is found that the ε″ values have an increase with the increase of MMT concentration in melt-compounded films, but the solution-cast films show the anomalous increase in their values.

AC conductivity spectra

Figure 3 shows that the real part of ac complex conductivity, σ′ of PEO–MMT nanocomposite films increases with the increase of frequency. Due to semicrystalline structures of PEO, the σ′(*f*) plots have two straight lines of different slopes (see inset of Figure 3 for pure PEO as a representative plot). The low frequencies straight line of σ′ has higher value of slope when compared with that of the high frequencies. Further, the σ′(*f*) values of pure PEO film are found in good agreement with the earlier reported data at same temperature.[23,39] The direct current conductivity σ_{dc} of these nanocomposite films were determined by straight line fit of low frequencies σ′ data. The evaluated σ_{dc} values are plotted against MMT concentration in the inset of Figure 3. It is found that the σ_{dc} values of PEO–MMT nanocomposite are low when compared with that of pure PEO film, and have maximum variation of nearly one order of magnitude around 2–3 wt % MMT loading in the PEO matrix. Inset of Figure 3 also includes the σ_{dc} values of aqueous solution-cast PEO–MMT films,[25] which are slightly high when compared with that of the melt-compounded films. It is expected because the solution-cast films may have some traces of polar solvent, which favors the ion-conduction mechanism. The peak in tanδ plots of Figure 3 are corresponding to PEO segmental motion and its loss tangent relaxation time $\tau_{\tan\delta}$ were determined from the tanδ peak frequency $f_{p(\tan\delta)}$ by the relation $\tau_{\tan\delta} = (2\pi f_{p(\tan\delta)})^{-1}$.

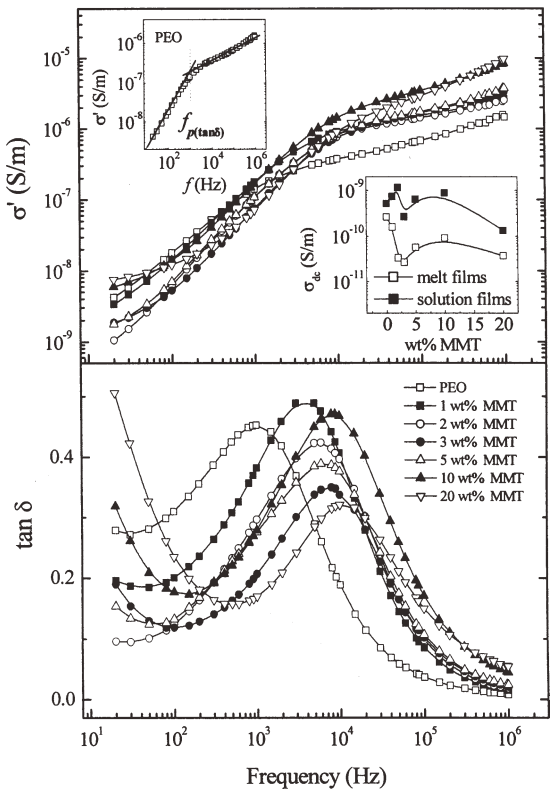

Figure 3 Frequency dependence of real part of ac conductivity σ′ and loss tangent tanδ of the melt-compounded PEO–MMT nanocomposite films at varying MMT concentration (wt %). Insets show the two straight lines in σ′ spectra of pure PEO film and the variation of σ_{dc} with MMT concentration of melt-compounded and aqueous solution-cast PEO–MMT films.

Electric modulus spectra

The real part *M*′ of electric modulus spectra have shoulders in low and high frequency region, whereas dispersion occurs in the mid-frequency region (Fig. 4). The electric modulus loss *M*″ spectra shows the peaks in the frequency range of *M*′ dispersion region. These peaks are assigned to the ionic conductivity relaxation coupled with PEO segmental motion. The PEO segmental dynamics electric modulus relaxation time τ_M of these materials were determined from the *M*″ peak frequency $f_{p(M'')}$ using the relation $\tau_M = (2\pi f_{p(M'')})^{-1}$.

Dielectric relaxation behavior

In Figure 5, frequency dependent ε″, tanδ, and *M*″ functions are plotted for 3 wt % MMT loaded PEO–MMT film as representative plots to compare the various relaxation peaks in different formalisms. It is found that $f_{p(M'')} > f_{p(\tan\delta)} > f_{p(\varepsilon'')}$ for these PEO–MMT nanocomposite films. The order of variations in these relaxation peaks suggests a modification in density function of the distribution of relaxation times by transformation from one formalism to another.

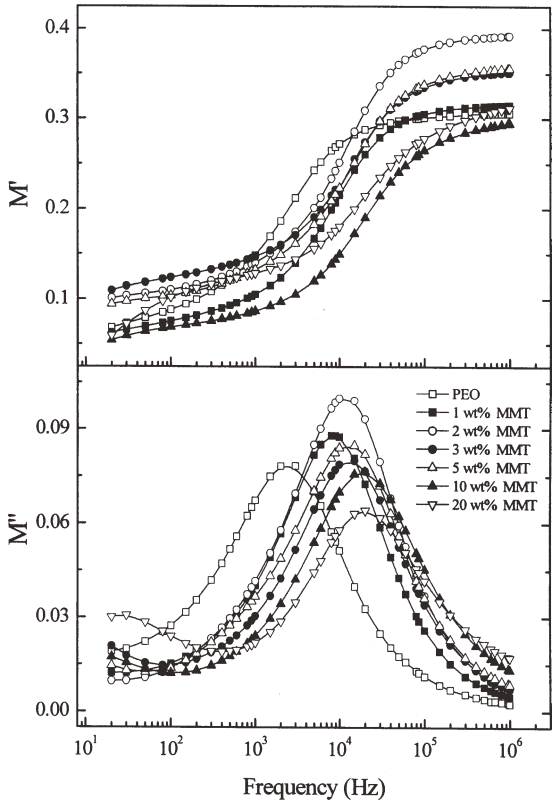

Figure 4 Frequency dependence of real part M' and loss M'' of electric modulus of the melt-compounded PEO–MMT nanocomposite films at varying MMT concentration (wt%).

Figure 6 shows the comparative values of τ_ε, $\tau_{tan\delta}$, and τ_M of the PEO–MMT nanocomposites, which have the order $\tau_\varepsilon > \tau_{tan\delta} > \tau_M$ at all the MMT concentration. Further, it is found that the relaxation times of PEO–MMT films evaluated from different formalisms have almost same trends in the variation of their values with the increase of MMT concentration. The relaxation time values of melt-compounded PEO–MMT nanocomposites are found low when compared with that of the pure PEO film, which

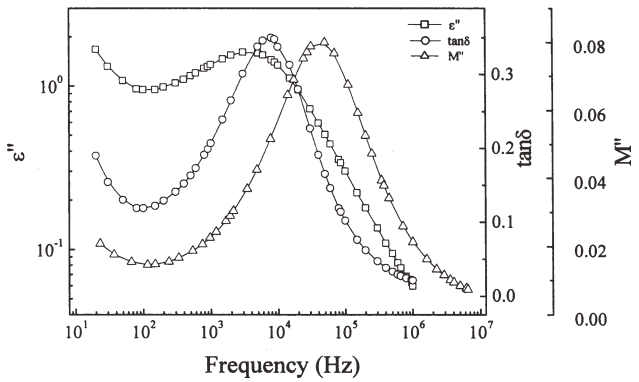

Figure 5 Comparative spectra of frequency dependent ε'', tanδ, and M'' of the melt-compounded PEO–MMT nanocomposite film of 3 wt % MMT concentration at ambient temperature.

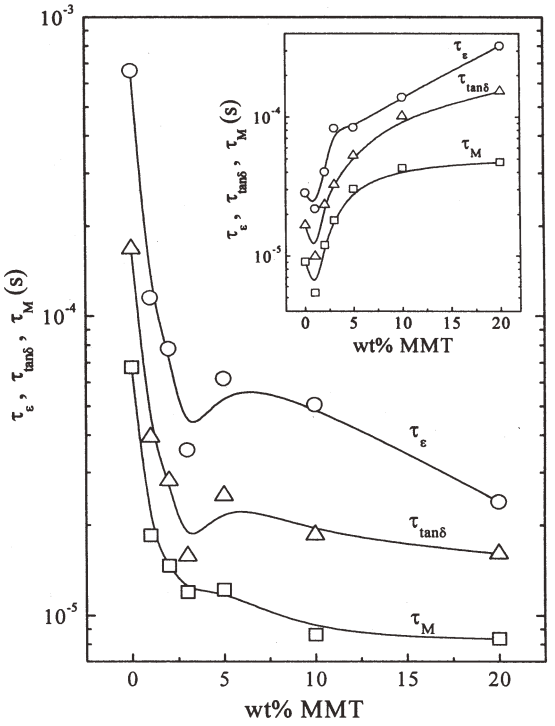

Figure 6 MMT clay concentration (wt %) dependence of PEO chain segmental motion dielectric relaxation time τ_ε, loss tangent relaxation time $\tau_{tan\delta}$, and electric modulus relaxation time τ_M of the melt-compounded PEO–MMT nanocomposite films at ambient temperature. Inset shows relaxation times of aqueous solution-cast PEO–MMT films. For clarity, errors bars are not indicated. Error bars are smaller than the size of symbols.

reveals significant increase in the PEO local chain dynamics when a small amount of MMT is loaded in PEO matrix. As confirmed from the XRD studies of these nanocomposites, the intercalated PEO in MMT galleries has an arrangement of the lamellar helical or multilayered *tgt* type nanostructures, which facilitate the PEO-segmental dynamics and hence there is decrease in the values of relaxation times at 1 wt % MMT concentration. The anomalous changes in relaxation times at higher MMT concentrations may be owing to the comparative variations in exfoliated/intercalated-MMT structures and their distributions in PEO matrix. Such structural changes affect the interactions between the PEO and dispersed MMT, and hence the PEO local chain dynamics.

The inset of Figure 6 depicted the relaxation times of aqueous solution-cast PEO–MMT films.[25] The order $\tau_\varepsilon > \tau_{tan\delta} > \tau_M$ of these solution-cast films is same as that of melt-compounded, but in contrast to melt-compounded nanocomposites, the solution-cast films have increase of relaxation times with the increase of MMT concentration in PEO matrix, except at 1 wt % MMT. This also confirms the differences in the molecular level interactions between PEO and MMT when synthesized by the dry route melt-compounded and solution-cast techniques.

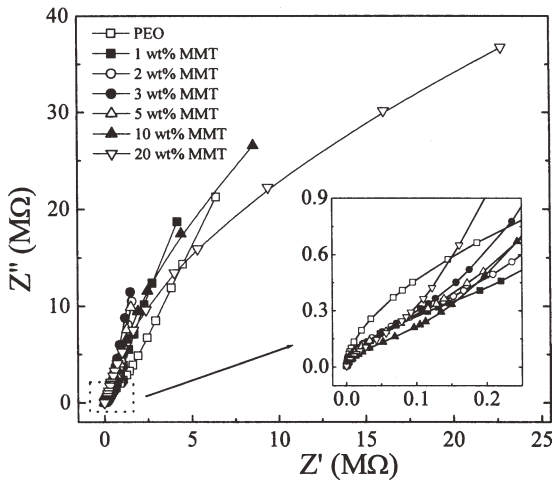

Figure 7 Complex impedance plane plots (Z'' versus Z') of the melt-compounded PEO–MMT nanocomposite films at varying MMT concentration (wt %). Inset shows the enlarged view in the high frequency region.

Further, the values of various relaxation times of solution-cast pure PEO film are about one order of magnitude lower than that of the melt-synthesized PEO film, which may be due to the presence of solvent traces in the solution-cast film. The trends of relaxation times values with increase of MMT loading of aqueous solution-cast and melt-compounded PEO–MMT nanocomposite films established the fact that the PEO dynamics and PEO–MMT complex structures are governed by their preparation route.

Impedance behavior

Figure 7 shows the impedance plane plots (Z'' versus Z'; Nyquist plots) of the melt-compounded PEO–MMT nanocomposites in which frequency of the experimental data points increases going from right to left on the arcs. These arcs have start from the origin and inclined at different angles to the real axis. The shape of these arcs gives the information regarding the electrode polarization (formation of electric double layers between electrodes and the dielectric material surfaces) and about the current carriers whether they are electrons or ions.[40,41] In general, ion-conducting materials show two distinct arcs in the impedance plane plots corresponding to the electrode polarization in low-frequency region and the bulk material properties in high-frequency region.[31,33] For these nanocomposite materials, the observed single arcs represent the bulk-material property, which implies that there is no contribution of electric double layers for charge transfer between the interface of material and the electrodes in the experimental-frequency range. The enlarged view of the impedance plots in high-frequency region is shown in the inset of Figure 7. The appearance of almost single arcs in the Z'' versus Z' plots also suggests the formation of a good electrical contact between the PEO–MMT films and the nickel-plated cobalt electrodes. The large values of Z'' when compared with the Z' confirm a high capacitive behavior of these nanocomposite films, which is owing to their low values of dc conductivity.

CONCLUSIONS

The manuscript presents the XRD and dielectric/electrical studies on MMT structures and PEO dynamics in melt-compounded PEO–MMT nanocomposites. XRD patterns confirm the formation of intercalated and exfoliated-MMT structures in these nanocomposites. The significant decrease of real part of dielectric function up to 5 wt % MMT concentration when compared with that of the pure PEO film revealed the predominance of exfoliated-MMT structures in the melt-compounded PEO matrix. The relaxation time values of these nanocomposites inferred that the PEO chain segmental dynamics enhances with the increase of MMT concentration due to formation of intercalated structures. The dc conductivity of these nanocomposite materials are lower than that of the pure PEO, and vary anomalously within one order of magnitude with increase of MMT concentration up to 20 wt %. The significant difference in values of ε' at 1 MHz, dc conductivity and relaxation time of the melt-compounded PEO–MMT nanocomposites when compared with that of the aqueous solution-cast materials establish the fact that MMT structural behavior and PEO local chain dynamics are affected by the nanocomposite preparation route.

Authors are grateful to the Department of Science and Technology, New Delhi for providing the dielectric experimental facilities through project No. SR/S2/CMP-09/2002 and the XRD facility in the DST–FIST program No. SR/FST/PSI-134/2008. One of the authors Shobhna Choudhary is thankful to the University Grants Commission, New Delhi for the award of RFSMS fellowship.

References

1. Ogata, N.; Kawakage, S.; Ogihara, T. Polymer 1997, 38, 5115.
2. Shen, Z.; Simon, G. P.; Cheng, Y. B. Polymer 2002, 43, 4251.
3. Shen, Z.; Simon, G. P.; Cheng, Y. B. Eur Polym J 2003, 39, 1917.
4. Strawhecker, K. E.; Manias, E. Chem Mater 2003, 15, 844.
5. Reinholdt, M. X.; Kirkpatrick, R. J.; Pinnavaia, T. J. J Phys Chem B 2005, 109, 16296.
6. Hikosaka, M. Y.; Pulcinelli, S. H.; Santilli, C. V.; Dahmouche, K.; Craievich, A. F. J Non-Cryst Solids 2006, 352, 3705.
7. Elmahdy, M. M.; Chrissopoulou, K.; Afratis, A.; Floudas, G.; Anastasiadis, S. H. Macromolecules 2006, 39, 5170.
8. Miwa, Y.; Drews, A. R.; Schlick, S. Macromolecules 2008, 41, 4701.

9. Noda, N.; Lee, Y. H.; Bur, A. J.; Prabhu, V. M.; Snyder, C. R.; Roth, S. C.; McBrearty, M. Polymer 2005, 46, 7201.
10. Mijović, J.; Lee, H.; Kenny, J.; Mays, J. Macromolecules 2006, 39, 2172.
11. Bur, A. J.; Lee, Y. H.; Roth, S. C.; Start, P. R. Polymer 2005, 46, 10908.
12. Wang, H. W.; Dong, R. X.; Liu, C. L.; Chang, H. Y. J Appl Polym Sci 2007, 104, 318.
13. Kortaberria, G.; Solar, L.; Jimeno, A.; Arruti, P.; Gómez, C.; Mondragon, I. J Appl Polym Sci 2006, 102, 5927.
14. Pissis, P.; Fragiadakis, D. J Macromol Sci B Phys 2007, 46, 119.
15. Bershtein, V. A.; Fainleib, A. M.; Pissis, P.; Bei, I. M.; Dalmas, F.; Egorova, L. M.; Gomza, Y. P.; Kripotou, S.; Maroulos, P.; Yakushev, P. N. J Macromol Sci B Phys 2008, 47, 555.
16. Pandis, C.; Logakis, E.; Peoglos, V.; Pissis, P.; Omastová, M.; Mravćáková, M.; Janke, A.; Pionteck, J.; Peneva, Y.; Minkova, L. J Polym Sci B Polym Phys 2009, 47, 407.
17. Sengwa, R. J.; Choudhary, S.; Sankhla, S. Express Polym Lett 2008, 2, 800.
18. Sengwa, R. J.; Choudhary, S.; Sankhla, S. Colloids Surf A Physicochem Eng Aspects 2009, 336, 79.
19. Sengwa, R. J.; Choudhary, S.; Sankhla, S. Polym Int 2009, 58, 781.
20. Sengwa, R. J.; Sankhla, S.; Choudhary, S. Colloid Polym Sci 2009, 287, 1013.
21. Sengwa, R. J.; Choudhary, S.; Sankhla, S. Indian J Eng Mater Sci 2009, 16, 395.
22. Sengwa, R. J.; Sankhla, S.; Choudhary, S. Indian J Pure Appl Phys 2010, 48, 196.
23. Sengwa, R. J.; Choudhary, S.; Sankhla, S. Compos Sci Tech 2010, 70, 1621.
24. Sengwa, R. J.; Choudhary, S. Express Polym Lett 2010, 4, 559.
25. Sengwa, R. J.; Choudhary, S. J Macromol Sci B Phys 2011, 50, 1313.
26. Wang, H. W.; Shieh, C. F.; Chang, K. C.; Chu, H. C. J Appl Polym Sci 2005, 97, 2175.
27. Kaya, A. U.; Esmer, K.; Takin, N.; Beyaz, S. K. J Appl Polym Sci 2011, 120, 874.
28. Cardoso, J.; Montiel, R.; Manero, O. J Appl Polym Sci 2011, 119, 1357.
29. Treichel, H.; Ruhl, G.; Ansmann, P.; Würl, R.; Müller, Ch.; Dietimeier, M. Microelectron Eng 1998, 40, 1.
30. Tanaka, T.; Montanari, G. C.; Mülhaupt, R. IEEE Trans Dielect Elect Insul 2004, 11, 763.
31. Choudhary, S.; Sengwa, R. J. Ionics 2011, doi: 10.1007/s11581-011-0585-8.
32. Huskic, M.; Zigon, M. J Appl Polym Sci 2009, 113, 1182.
33. Mohapatra, S. R.; Thakur, A. K.; Choudhary, R. N. P. J Power Sources 2009, 191, 601.
34. Ragavendran, K.; Kalyani, P.; Veluchamy, A.; Banumathi, S.; Thirunakaran, R.; Benedict, T. J. Portugaliae Electrochim Acta 2004, 22, 149.
35. Chen, H. W.; Chang, F. C. Polymer 2001, 42, 9763.
36. Aranda, P.; Mosqueda, Y., Perez-Cappe, E.; Ruiz-Hitzky, E. J Polym Sci B Polym Phys 2003, 41, 3249.
37. Chen, B.; Evans, J. R. G. J Phys Chem 2004, 108, 14986.
38. Tunney, J. J.; Detellier, C. Chem Mater 1996, 8, 927.
39. Mishra, R.; Rao, K. J. Solid State Ionic 1998, 106, 113.
40. Macdonald, J. R. Impedance Spectroscopy, Emphasizing Solid Materials and Systems; Wiley: New York, 1987.
41. Kremer, F.; Schönhals, A. Broadband Dielectric Spectroscopy, Springer-Verlag: New York, 2003.